Nanoscale

Accepted Manuscript

This article can be cited before page numbers have been issued, to do this please use: V. Bordoni, G. Reina, M. Orecchioni, G. Furesi, S. Thiele, C. Gardin, B. Zavan, G. Cuniberti, A. Bianco, M. Rauner and L. G. Delogu, *Nanoscale*, 2019, DOI: 10.1039/C9NR03975A.

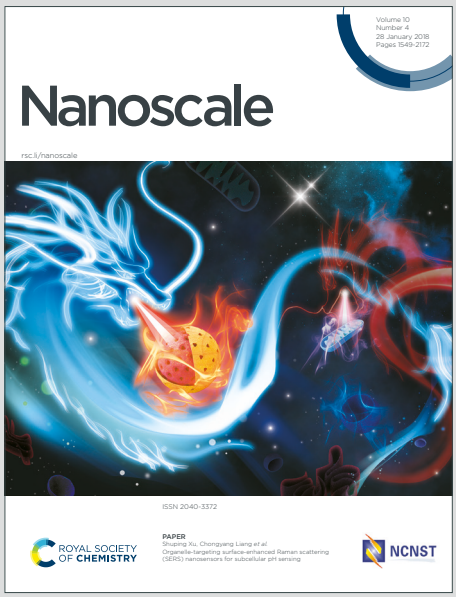

ROYAL SOCIETY OF CHEMISTRY

rsc.li/nanoscale

View Article Online
DOI: 10.1039/C9NR03975A

Stimulation of bone formation by monocyte-activator functionalized graphene oxide *in vivo*

Valentina Bordoni[1#], Giacomo Reina[2#], Marco Orecchioni[1#], Giulia Furesi[1,3], Stefanie Thiele[3], Chiara Gardin[4], Barbara Zavan[4], Gianaurelio Cuniberti[5], Alberto Bianco[2], Martina Rauner[3*], and Lucia G. Delogu[1,6,7*]*

[1] University of Sassari, Sassari, Italy
[2] University of Strasbourg, CNRS, Immunology, Immunopathology and Therapeutic Chemistry, UPR 3572 Strasbourg, France
[3] TU Dresden Medical Center, Dresden, Germany
[4] Department of Biomedical Sciences University of Padova, Padova, Italy
[5] Max Bergmann Center of Biomaterials and Institute for Materials Science, Dresden University of Technology, Dresden, Germany
[6] Center for Advancing Electronics Dresden, TU Dresden, Dresden, Germany
[7] Fondazione Istituto di Ricerca Pediatrica Città della Speranza, Padova, Italy

Corresponding authors:

a.bianco@ibmc-cnrs.unistra.fr, Martina.Rauner@uniklinikum-dresden.de, lgdelogu@uniss.it

[#] These authors contributed equally to this work

Keywords

Carbon nanomaterials, graphene, complexes, bone, immune response, osteoblasts.

Abstract

Nanosystems are able to enhance bone regeneration, a complex process requiring the mutual interplay between immune and skeletal cells. Activated monocytes can communicate pro-osteogenic signals to mesenchymal stem cells and promote osteogenesis. Thus, the activation of monocytes is a promising strategy to improve bone regeneration. Nanomaterials specifically selected to provoke immune-mediated bone formation are still missing. As a proof of concept, we apply here the intrinsic immune-characteristics of a specific graphene oxide (GO) with the well-recognized osteoinductive capacity of calcium phosphate (CaP) in a biocompatible nanomaterial called maGO-CaP (monocytes activator GO complexed with

View Article Online
DOI: 10.1039/C9NR03975A

CaP). In the presence of monocytes, the alkaline phosphatase activity and the expression of osteogenic markers increased. Studying the mechanisms of action, we detected an up-regulation of Wnt and BMP signaling, two key osteogenic pathways. The role of the immune activation was evidenced by the over-production of Oncostatin M, a pro-osteogenic factor produced by monocytes. Finally, we tested the pro-osteogenic effects of maGO-CaP *in vivo*. maGO-CaP injected into the tibia of mice enhanced local bone mass and the bone formation rate. Our study suggests that maGO-CaP can activate monocytes to enhance osteogenesis *ex vivo* and *in vivo*.

View Article Online
DOI: 10.1039/C9NR03975A

1. Introduction

One of the main challenges in regenerative medicine is the development of new strategies to improve bone health and the quality of life in patients with bone injuries and diseases. [1,2] Bone regeneration is a complex process that involves the spatial and temporal coordination of many biological events. [3] Osteogenesis is based on the development of new bone tissue by osteoblasts, derived from mesenchymal stem cells (MSCs).

The emerging field of osteoimmunology has elucidated the different biological processes and the molecules that intimately link the functions of bone and the immune system, including shared cytokines, receptors, signaling molecules and transcription factors. [4,5]

Activated immune cells, and in particular monocytes, produce soluble factors, which can strongly promote osteogenic gene expression and differentiation of MSCs. [6] Monocytes are among the first responders to tissue injury and are required for successful tissue regeneration. [7,8] During bone injury, monocytes and macrophages play crucial roles in maintaining bone homeostasis and promoting fracture repair through the modulation of the acute inflammatory response, the production of growth factors, and the improvement of the differentiation of mesenchymal progenitors. [9,10,11]

In bone tissue engineering, the therapeutic strategies based on nanomaterials have seen recent progress on several fronts. [12] These strategies were employed to boost osteogenesis and create scaffolds with higher osseointegration and osteoconduction proprieties. [13,14,15] In this context graphene displays unique physicochemical properties, such as a large surface area, [16] a well-established surface chemistry, [17] and superior mechanical strength. [18,19] Recent *in vitro* studies have shown that graphene oxide, one of the most explored graphene-based materials, facilitates osteoblast differentiation of MSCs and enhances bone regeneration without causing any relevant toxicity. [20, 21, 22, 23, 24, 25, 26] Depending on their chemicophysical properties, graphene family materials can be selected for exerting distinct molecular effects on

the immune cells. [27, 28, 29] These intrinsic immune properties of specific graphenic materials will be of advantage for new immune-based strategies in osteogenesis and bone regeneration. We recently demonstrated that a particular type of GO with a small lateral dimension (<1 μm) is able to induce specific activation of monocytes. [30] Although the role of immune cells in bone regeneration in the presence of nanomaterials has not been elucidated yet, an appropriate GO might activate immune cells and stimulate bone formation. [31]

Based on these considerations, we have selected graphene oxide to explore its potential for bone formation. We have combined the specific activation properties of GO on monocytes [30] and the well-recognized osteoinductive capacity of calcium phosphates (CaP) [32,33] to develop an advanced nanomaterial called maGO-CaP (monocyte activator graphene oxide conjugated with calcium phosphates). In this study, we have analyzed the effect of maGO-CaP on osteogenic differentiation of human primary MSCs (hMSCs) co-cultured with human primary monocytes *ex vivo* and *in vivo* in mice. Firstly, we proved the high biocompatibility of maGO-CaP on hMSCs and monocytes by analyzing cell viability and metabolism. We verified the monocyte activation action of maGO-CaP by flow cytometry and ELISA. In the presence of monocytes, the strong ability of the material to induce the osteogenesis was assessed by measuring the amount of calcium deposits, the alkaline phosphatase activity and through the expression of several osteogenic markers. Exploring the possible mechanisms, we revealed the up-regulation of two main actors in osteoblastogenesis: Wnt and BMP signaling pathways (**Scheme 1**). Moreover, the correlation between the osteogenic potential of maGO-CaP and the role of the immune activation was evidenced by the over-production of oncostatin M, a pro-osteogenic factor produced by monocytes. Finally, the animal study showed the non-toxicity of maGO-CaP and validated that our material was able to successfully facilitate the bone formation *in vivo*.

View Article Online
DOI: 10.1039/C9NR03975A

2. Results and discussion

2.1 Synthesis of maGO-CaP, cell viability and metabolism

First, CaP were prepared following a protocol reported in the literature CaP amorphous nanoparticles were obtained via the reverse emulsion method using Pluronic F127 as capping agent. [21] maGO-CaP were then synthesized by adding the GO flakes to CaP nanoparticles. Subsequently, mature CaP and maGO-CaP were obtained storing the samples in deionized water for 20 days. Freshly synthetized CaP are round nanoparticles with a diameter of 18 ± 4 nm (**Figure S1A**). The presence of GO did not alter CaP morphology or size (17 ± 3 nm) (**Figure S1B**), while the particles appears mostly adsorbed onto the GO surface. Ca/P ratio (estimated by XPS) showed similar values both for immature CaP and maGO-CaP (1.1 and 1.3, respectively) (**Figure S1C**). The maturation process dramatically changes the morphological and structural features of the CaP nanoparticles. TEM analysis evidenced the CaP as oblong plated shapes with the mayor length of 80 ± 20 nm and a CaP thickness in the order of a few nanometers (**Figure 1, A1**). When GO is present in the maturation solution, the formed calcium phosphate nanoparticles show the same morphology of isolated CaP but with a slightly shorter length (60 ± 20 nm) (**Figure 1, A2**). The Raman characterization of CaP shows the typical band of PO_4^{-3} ν1 at 960 cm^{-1} (**Figure S1D**). maGO-CaP spectrum revealed the co-existence of both GO and CaP, with the strong peak of the phosphate (960 cm^{-1}) as well as the D (1330 cm^{-1}) and G bands (1597 cm^{-1}) of GO (**Figure S1D**). Interplanar spacing was calculated from the selective electron diffraction (SAED) area as described in the Methods. CaP lattice structure evidences the typical hydroxyapatite pattern with reflections at 0.355, 0.284 and 0.178 nm attributed to the [002], the overlapped [210] and [211], and the [004] lattice planes, respectively (**Figure S1E**). [34,35] In the case of maGO-CaP, SAED characterization displayed the presence of GO with a halo attributed to the [110] at 0.148 nm, corresponding to the GO C-C spacing (**Figure S1F**). [36] In addition, the calcium phosphate

View Article Online
DOI: 10.1039/C9NR03975A

reflections are more marked with the appearance of new diffraction intensities at 0.202 and 0.189 nm attributed to [222] and [312] lattice planes.

To date, several studies both *in vitro* and *in vivo* reported contradictory results about graphene biocompatibility. [37] Some manuscripts have described good biocompatibility with no impairment of cell viability, [38,39] while others have evidenced increased cell apoptosis and necrosis after GO exposure. [40,41] As the impact of graphene materials on cells likely depends on several factors including lateral size dimension, shape, thickness, stiffness, surface functionalization, concentration and time of exposure to cells [42] we first characterized the biocompatibility of maGO-CaP.

Monocytes were isolated from human peripheral blood mononuclear cells (PBMCs) and exposed to GO, maGO-CaP or CaP at 5, 25 and 50 μg/ml. AnnexinV/propidium iodide (PI) staining were used to assess early apoptosis, late apoptosis and necrosis (**Figure 1B**). We did not detect any significant differences in the percentage of apoptotic and necrotic cells compared to the control samples, even at the highest concentration (50 μg/ml) (**Figure 1B**). The flow cytometry profile has shown similar profiles for early apoptotic, late apoptotic and necrotic cells between the controls and the treated samples (**Figure S2**). Furthermore, we confirmed by the CellTiter Blue assay that the exposure to increasing doses (5, 25, 50 μg/ml) of maGO-CaP did not affect the monocyte viability (**Figure 1C**).

Annexin V/PI staining and CellTiter Blue assay were performed also on hMSCs. Similarly, maGO-CaP did not affect cell viability (**Figure 1D** and **E**). Our results agree with those of other authors who reported a good biocompatibility of graphene-based materials on MSCs. [43,44] For example, Zancanela et al. reported that GO does not affect the viability of osteoblasts after 5 days of incubation using concentrations of 25 and 50 μg/ml. [45]

Then we performed hematopoietic analysis by evaluating the impact of GO, CaP and maGO-CaP on human PBMCs obtained from healthy donors. We evaluated the main immune cell populations (*e.g.* T cells, B cells, natural killer cells and monocytes), responsible of the *in vivo*

View Article Online
DOI: 10.1039/C9NR03975A

immune response. [46,47] We did not find any toxicity on PBMCs after treatment with each material at each concentration (2.5, 5, 25, 50 and 100 μg/ml) (**Figure S3**).

2.2 maGO-CaP innate immune function

Activated monocytes were shown to stimulate the function of osteoblasts. [4,5,6] Since we previously have discovered the ability of a selected GO to activate monocytes, [30] we first validated the ability of maGO-CaP, derived from the same type of GO, to boost an innate response. Monocytes were isolated from PBMCs and incubated for 24 h with GO or maGO-CaP (5, 25, 50 μg/mL) or left untreated. The expression of immune activation markers (cluster of differentiation [CD]) CD69, CD25 and CD80 was evaluated by flow cytometry (**Figure 2A**). CD69, a member of the C-type lectin superfamily (Leu-23), is one of the earliest inducible cell surface glycoproteins expressed by immune cells during activation. CD25 is the alpha chain of the IL-2 receptor, a late activation antigen expressed by lymphomonocytes. CD80 is a protein found on activated antigen presenting cells that play an important role in T cell activation and survival.

All investigated activation markers were highly induced after 24 h of treatment by GO. Therefore, we confirmed its activation action on monocytes (**Figure 2A**). maGO-CaP maintained the same functionality of GO, with a statistically significant induction of CD25 andCD80 (P value < 0.01) (**Figure 2A**). The activation of monocytes was further confirmed by measuring the levels of TNFα and IL-6 in the cell culture media (**Figure 2B**). IL-6 and TNFα are normally secreted by monocytes/macrophages and their action is related to the innate immune system response. In our previous work, we evaluated the effect of GO on immune cells, observing at the genome level a particular enhancement of the expression of specific genes relative to the production of IL-6, IL-10, TNFα and CD80. [30] In the same way, Zhi et al. showed that the incubation with GO induced a specific activation of the innate

immune system with a secretion of primary proinflammatory cytokines such as IL-6, TNFα and IL1β. [48]

To investigate the possibility that other immune cells were affected by the maGO-CaP treatment, we evaluated the impact of GO and maGO-CaP on the main immune cell populations (T cells, B cells, NK cells, and monocytes) to monitor their activation status. We found an overexpression of CD69, CD25, and CD80 on monocytes, while T cells, B cells and NK cells were not affected by maGO-CaP treatment (**Figure S4**). The monocyte activation status was evident at 50 μg/ml and it was maintained at the concentration of 100 μg/ml, with a similar expression of activation markers between these two concentrations. However, based on previous studies carried out by us and others, we decided to used 50 μg/ml in the following experiments as the ideal concentration for potential biomedical use of graphene. [27,30,49]

2.3 maGO-CaP promotes osteoblast differentiation in the presence of monocytes

Monocytes were shown to stimulate MSC differentiation into osteoblasts by producing pro-osteogenic factors, such as oncostatin M (OSM), and by activating osteoblasts through direct cell contacts. [7,50,51] The prolonged stimulation of monocytes by maGO-CaP could promote the release of pro-osteogenic mediators, which induce an osteogenic response in hMSCs. To test this hypothesis, we exposed a co-culture of human monocytes and hMSCs to GO, CaP and maGO-CaP at 50 μg/ml, concentration able to induce osteoblast differentiation. Alkaline phosphatase (ALP) activity was measured to evaluate the osteogenic properties of maGO-CaP (**Figure 3A**). ALP is a hydrolase enzyme involved in the dephosphorylation process of many types of molecules and it is an important component in hard tissue formation. The increase of its activity is an index of the differentiation of stem cells into osteoblastic lineage. [52,53,54,55,56] ALP staining and quantification of its activity revealed an increase of ALP activity in maGO-CaP-treated cells compared to negative controls and samples treated with only CaP (p

View Article Online
DOI: 10.1039/C9NR03975A

value<0.001) (**Figure 3A**). maGO-CaP osteogenic properties were confirmed by the analysis of bone matrix formation via alizarin red S assay after 14 days of co-culture (**Figure 3B**). Following the treatment with maGO-CaP (50 μg/ml), the enhancement of bone nodule formation was evident in relation to the control and CaP alone (**Figure 3B**). In hMSC cultures without monocytes, the osteogenic potential of maGO-CaP was reduced as compared to co-culture (**Figure S5**). We can assume that maGO-CaP have a direct effect on hMSCs mediated by the presence of CaP, plus an indirect effect on monocytes mediated by GO that significantly boost osteoblastogenesis in the co-culture experiments. Based on these results, we propose that maGO-CaP play synergetic effects with monocytes in accelerating hMSCs differentiation toward osteoblast lineage.

To verify the pro-osteogenic capacity of maGO-CaP, the expression of runt-related transcription factor (Runx2), collagen type 1 (Col1a), osteocalcin (OCN) and bone morphogenic proteins 6 (BMP6), key osteogenic genes, was investigated in the co-culture (**Figure 3C**). Osteoblasts arise from MSCs and their differentiation is promoted by two key pathways: the Wnt signaling pathway and BMP pathway. The activation of both pathways leads to the stimulation of osteoblastic transcription factors such as Runx2, a member of transcription factors family that induces the expression of osteoblast marker genes such as Col1a and OCN. Col1a1 and Col1a2 are the most abundant extracellular matrix (ECM) proteins in bone and play an important role in bone formation by triggering the expression of osteoblastic phenotypes through extracellular signals. OCN also called bone gamma-carboxyglutamic acid-containing protein (Bglap) is secreted by osteoblasts and is implicated in bone mineralization and calcium-ion homeostasis. We found a relevant over-expression of Runx2 and Col1a after two-week exposure to 50 μg/ml maGO-CaP compared to untreated samples (p value<0.001) and to samples treated with CaP (p value<0.01) (**Figure 3C**). Moreover, we found an up-regulation of OCN and BMP6 mediated by maGO-CaP compared to control samples (**Figure 3C**). Recent studies suggest the ability of graphene to stimulate

View Article Online
DOI: 10.1039/C9NR03975A

the gene and protein expression of Runx2, Col1 and OCN without any chemical inducers [57,58] Our data on maGO-CaP confirmed these properties of graphene, in view of the crosstalk between monocytes and bone cells.

2.4 maGO-CaP osteogenesis mechanisms

To investigate the possible mechanisms involved in the osteogenesis of maGO-CaP, we first evaluated the expression of specific genes involved in the Wnt pathway (**Figure 4A**). Wnt signaling pathways are a group of signal transduction pathways, highly conserved through evolution, implying a series of proteins involved in numerous aspects of growth and development of the bone. [59] Wnt signaling is separated into the canonical route that depends on the function of β-catenin (Wnt/β-catenin pathway) and the non-canonical pathway that operates independently of β-catenin (the planar cell polarity pathway and the Wnt/Ca^{2+} pathway). Wnt/β-catenin pathway involves numerous receptors, inhibitors, activators, modulators, phosphatases, kinases and other components that determine the rate of bone formation through different processes including stem cell regeneration, stimulation of pre-osteoblast replication, induction of osteoblastogenesis, and inhibition of osteoblast and osteocyte apoptosis. [60]

In this context, we verified the expression of the typical target genes of Wnt signaling, namely axin inhibition protein 2 (Axin2), CD44 and lymphoid enhancer-binding factor 1 (LEF1) in a co-culture of hMSCs and monocytes (**Figure 4A**). [61] The Axin2 plays an important role in the regulation of β-catenin stability in the Wnt signaling. [62] CD44 antigen is a cell-surface glycoprotein involved in cell-to-cell interactions, cell adhesion and migration. It is also a receptor for hyaluronic acid partially activated by β-catenin and Wnt signaling. [63] LEF1 activates several transcription factors through a Wnt/ β-catenin signaling, and participates in the Wnt signaling pathway activating transcription of target genes. [64]

View Article Online
DOI: 10.1039/C9NR03975A

We found a statistically significant up-regulation of Axin2 (p value<0.05), CD44 (p value<0.05) and LEF1 (p value<0.01) after exposure to 50 μg/ml maGO-CaP, thus demonstrating that its osteoanabolic action is associated with an up-regulation of the Wnt pathway (**Figure 4A**). The different expression of these genes between GO, CaP and maGO-CaP treatment is likely related to the intrinsic properties of maGO-CaP complex. maGO-CaP combines the ability of GO to stimulate the monocytes and the osteoinductivity properties of CaP on hMSCs. At the same time, maGO-CaP is endowed of new characteristics able to interact in a unique way with cells, activating specific pathways, such as the Wnt pathway, indicating a synergistic and incremented osteo and immune actions of calcium phosphate and GO when combined.

To have a broader overview on the impact of the key pathways involved in the pro-osteogenic effects of maGO-CaP, we used a PCR array to assess the expression profile of 84 key genes related to: i) bone formation, ii) bone mineral metabolism, and iii) cells growth, proliferation and differentiation. The heat map shows a strong up-regulation of specific bone-genes in response to maGO-CaP treatment as compared to untreated controls (**Figure 4B**). The heat map tables of the gene values examined are reported in **Figure S6**. Highly up-regulated genes included genes of the BMP pathway, which is associated to the development of bone mineralization. In particular, we found a significant increase in BMP2 expression with a fold change of 4.71, BMP3 (4.31-fold), BMP4 (2.12-fold), BMP6 (2.26-fold) and BMP7 (2.38-fold) (**Figure 4B** and **S6**). Interestingly, maGO-CaP treatment also up-regulated the expression of Smad1 (Mothers against DPP Homolog 1), which is an intracellular downstream effector of BMP signaling (**Figure 4B** and **6S**). Furthermore, several collagen genes associated to the ECM, which is a central component of the cellular microenvironment, including Col10a1 (4.36-fold change), Col14a1 (3.22-fold change), Col1a2 (2.85-fold change) were strongly up-regulated by maGO-CaP, confirming its pro-osteogenic potential (**Figure**

4B and **S6**). The results of the array are in agreement with the expression of the genes involved in the osteoblast differentiation (**Figure 3C**).

There is increasing evidence that OSM is one of the mediators released by activated monocytes able to stimulate osteogenesis in hMSCs. [50,51] Indeed, OSM is considered one of the major cytokines produced by activated monocytes/macrophages able to enhance bone formation *in vitro* and *in vivo*. [51,65] The enhanced osteogenesis has not been observed in correlations with others cytokines or mediators, such as IL-4, IL-10, IL-8 and TGFb. [50, 51] Several pieces of evidence suggest that OSM has anti-adipogenic properties involved in osteogenic differentiation of hMSCs. [66, 67] It has been also found that OSM is expressed in macrophages during intramembranous fracture healing, mainly during the early inflammatory phase, acting on the recruitment, proliferation, and/or osteoblast differentiation of endosteal mesenchymal progenitor cells and sustaining bone formation. [68]

Moreover, monocyte depletion or OSM conditional knockout mice have a reduced number of osteoblasts at the injury site. [68] After treatment with clinically used anabolic drugs the osteopenia is not rescued. [69] In addition, when monocyte infiltration is blocked, the local proliferation of macrophage increases. [70] These observations support to the conclusion that the secretion of OSM by activated monocytes/macrophages plays a key role in the promotion of bone formation in early stages of fracture healing. [71]

On these premises, we decided to evaluated whether OSM signaling was involved in the pro-osteogenic effects of maGO-CaP. For this experiment, we employed a OSM neutralizing antibody added to the co-culture at the concentration of 100 ng/ml (**Figure S7A**). Using alizarin red Staining, we observed a reduction of bone nodule formation in the presence of maGO-CaP and the OSM neutralizing antibody, suggesting a key role played by OSM in the differentiation of hMSCs into osteoblasts. To further confirm this finding, we performed an ELISA assay on supernatants of hMSC-monocyte co-cultures, 7 days post-seeding. OSM levels were significantly higher (p value < 0.0001) when hMSCs-monocytes were grown in

View Article Online
DOI: 10.1039/C9NR03975A

presence of 50 μg/ml of maGO-CaP respect to the untreated control condition (**Figure 5A**). This result suggests that the higher production of OSM by maGO-CaP treatment by co-cultured monocytes can positively affect the osteogenesis process. TLRs are a class of proteins playing a key role in the innate immune system [72] and graphene might elicit a TLR-mediated innate response. Graphene and GO-induced autophagy and activation was observed in macrophage cell lines and was dependent on TLRs, such as TLR4. [73,74,75] Recently, few layers graphene was shown to induce necrotic pathways in neoplastic monocytes partly through the interaction with TLR2. [76] To determine whether TLR2 and TLR4 are also required for the activation of monocytes by maGO-CaP, cells were pre-treated with anti-TLR2 and anti-TLR4 antibodies before incubation with maGO-CaP (50 μg/ml). In TRL4 pre-treated monocytes, we found a decrease of the expression of CD69, CD25 and CD80 compared to TLR2 pre-treated samples (**Figure S7B**). We evaluated then the expression of OSM in the co-culture pre-treated with anti-TLR2 and anti-TLR4 antibodies (**Figure 5B** and **C**). No differences in OSM levels were measured in the cell culture media of pretreated anti-TLR4 cells, therefore suggesting that TLR4 is involved in monocyte activation. But maGO-CaP still promoted the secretion of OSM after anti-TLR2-pretreatment, suggesting that TLR2 does not mediate maGO-CaP actions (**Figure 5B**). Several studies suggested that the activation of TLRs by exogenous or endogenous ligands stimulates the production of OSM from monocytes, enhancing bone formation. [50, 77, 78] All together, these observations suggest that TLR4 is involved in the monocyte activation mediated by maGO-CaP and correlated to the release of OSM during the osteogenic process. To evaluate the role of TLRs in monocyte activation and their correlation with osteogenesis, we performed alizarin red staining to visualize the formation of the bone matrix. In accordance to OSM expression, we observed a significant increase of bone nodules in the samples incubated with maGO-CaP and pretreated with anti-TLR2 compared to controls (p value<0.01) (**Figure 5C**). The pre-treatment with anti-TLR4 before maGO-CaP exposure reduced the stimulation of bone matrix formation

View Article Online
DOI: 10.1039/C9NR03975A

compared to samples pre-treated with anti-TLR2. These data suggest that activation of monocytes by maGO-CaP is partly mediated by TLR4, therefore affecting the osteogenesis process.

2.5 maGO-CAP bone formation *in vivo*

To investigate whether maGO-CaP was able to exert osteoblast-promoting effects *in vivo*, we injected 50 µg/ml maGO-CaP or PBS into the tibia of healthy, 12-week-old C57BL/6 male mice. First, we investigated the *in vivo* biocompatibility and the possible systemic inflammation (**Figure S8**). maGO-CaP was well tolerated 7 days and 1 month after injection. There was no difference in the percentage of inflammatory cells present in the spleen, the lymph nodes, the thymus and the bone marrow between the mice treated with maGO-CaP or with PBS (**Figure S8**). Thus, the localized injection does not lead to significant differences in the percentage of inflammatory cells. These results on systemic inflammation support the hypothesis that maGO-CaP, after intratibial injection, might induce only a local effect without causing system inflammation.. The blood count reported in **Table S1** shows that the number of white blood cells were also not affected by maGO-CaP treatment. Indeed, treated and untreated mice presented similar value of hematopoietic cells, suggesting that maGO-CaP is well tolerated and does not trigger systemic inflammation (**Figure S9**). Finally, the macroscopic analysis of the internal organs of the mice treated with maGO-CaP did not show any aberrations (data not shown). Thus, the local application of maGO-CaP was well tolerated by the animals after one month from the injection.

To assess maGO-CaP osteogenic potential *in vivo*, three-dimensional µCT measurements of the tibias were performed (**Figure 6A)**. Trabecular bone volume fraction (BV/TV) significantly increased by maGO-CaP treatment (p value<0.01). The µCT image, representative of maGO-CaP treatment, shows the boost of the bone formation (**Figure 6A**). Furthermore, we detected differences in bone characteristics: a statistically significant (p

View Article Online
DOI: 10.1039/C9NR03975A

value<0.05) increase of the trabecular number (Tb.N) and the trabecular thickness (Tb.Th) was found in the tibias of mice treated with maGO-CaP (**Figure S10**). To verify whether the increased bone volume fraction was mediated by an increased bone formation or by a decreased bone resorption, we determined the number of osteoblasts and osteoclasts using histology. The number of osteoclasts, which are large multinucleated cells responsible for bone resorption, was not affected by maGO-CaP treatment. However, the number of osteoblasts per bone perimeter was significantly (p value<0.05) increased in maGO-CaP-treated mice (**Figure 6B**). In line with this observation, dynamic bone histomorphometry revealed an increase of mineralized surface, indicating more osteoblasts per bone surface (p value<0.05) (**Figure 6C**). In addition, the bone formation rate was enhanced (p value<0.05) in mice treated with maGO-CaP compared to the control group (**Figure 6C**).

Fianlly, we evaluated the impact of maGO-CaP on gene expression of the total bone marrow (**Figure 6D** and **S11**). We performed an osteogenesis array on bone marrow cells investigating the expression of 84 bone formation-related genes. Similarly to the *ex vivo* experiments, we found an over-expression of collagens associated with extracellular matrix, including Col1a1 (2.85-fold), Col1a2 (4.16-fold), biglycan (Bgn 2.66-fold change), and osteocalcin (Bglap 2.20-fold change) (**Figure 6D** and **S11**). Taken together, these data demonstrate that the bone-increasing effect of maGO-CaP *in vivo* is mediated *via* an increased activity of osteoblasts.

3. Conclusions

Considering the key role of immune cell-derived factors on bone formation by graphene, we demonstrated that biocompatible maGO-CaP exerts excellent pro-osteogenic properties. By looking at the mechanism of maGO-CaP action, we have shown the activation of Wnt, bone formation and collagen pathways. These main actors on osteoblast differentiation were identified together with a significant induction of oncostatin M, a key molecule involved on

View Article Online
DOI: 10.1039/C9NR03975A

monocyte-driven osteogenesis. Furthermore, the enhanced bone formation action of maGO-CaP was confirmed *in vivo*, in intratibially injected mice, by μCT analysis, histology and fluorescence microscopy. Our pre-clinical investigations demonstrate that appropriately functionalized graphene offers real medical opportunities to fight bone-related disorders. Moreover, we believe that our osteoimmune-approach can shape the entire research field of nanomaterials for bone regeneration.

4. Experimental Section

Materials

All reagents were purchased from Sigma Aldrich. The solvents were obtained from commercial suppliers and used without purification. Water was purified using a Millipore filter system MilliQ® and free endotoxin Polisseur Biopak®. GO was purchased from NanoInnova (Spain) (batch no. NIT.GO.R.10.1) as a powder. This GO was produced by a modified Hummers' method. It was characterized by the typical XRD pattern of GO and a highly oxidized surface (O/C ratio of 0.45) as described in the datasheets provided by the company.

Instruments

Raman analysis was performed using Raman spectra Renishaw inVia micro- Raman equipped with 514 nm laser and a Leica microscope. All spectra were recorded with 5% laser power using ×50 objective lens. The samples for Raman analysis were prepared by drop-casting 10 μL of the respective samples on Si window (ThorLabs) and dried for 24 h at room temperature.

TEM images were performed with Hitachi H7500 microscope (Tokyo, Japan) with an accelerating voltage of 80 kV, equipped with an AMT Hamamatsu camera (Tokyo, Japan). HR-TEM and SAED analyses were performed with a JEOL 2100F TEM/STEM electron

View Article Online
DOI: 10.1039/C9NR03975A

microscope operating at 200 kV. Interplanar spacing (d) was calculated from SAED according to the formula d= 2/(distance between two bright spots).

X-ray Photoelectron Spectroscopy (XPS) analyses were performed on a Thermo Scientific K-Alpha X-ray photoelectron spectrometer with a basic chamber pressure of 10^{-8}–10^{-9} bar with an anode using Al Kα radiation (hν = 1486.6 eV). The samples were analyzed as powders. A spot size of 400 μm was used. The survey spectra are the average of 10 scans with a pass energy of 200.00 eV and a step size of 1 eV.

Synthesis and characterization of maGO-CaP

CaP and maGO-CaP were synthesized according to the literature by mixing two reverse microemulsions A and B. [18] Emulsion A was prepared by mixing 200 μL of 100 mM $CaCl_2$, in 2.65 ml of 30% Igepal CO-520 in cyclohexane. Emulsion B was prepared by mixing 200 μL of 60 mM Na_2HPO_4 in 2.65 ml of 30% Igepal CO-520 with 50 μl of DMF. For the preparation of maGO-CaP, 1 mg of GO was added to the phosphate solution before adding cyclohexane. Both emulsion A and B were stirred for 30 min till the formation of a clear microemulsion. Then the microemulsion B was added dropwise under vigorous stirring to the microemulsion A (affording microemulsion C) and stirred for 5 min. Subsequently, 50 μl of 1% Pluronic® F-127 solution in water was slowly added dropwise to the microemulsion C and the microemulsion was left under stirring for 30 min. Then, 16 ml of ethanol were added to destroy the emulsion and the CaP or maGO-CaP were separated via centrifugation (5000 rpm, 10 min) and washed three times with ethanol and three times with water. Finally, the CaP and maGO-CaP were kept in milliQ water (10 ml) for 20 days for maturation.

Cell culture, apoptosis and viability assay

Buffy coats from healthy blood donors were obtained from the University Hospital Carl Gustav Carus, Dresden, and PBMCs were purified by biocoll gradient centrifugation (1.077

View Article Online
DOI: 10.1039/C9NR03975A

g/ml, Biochrom). Monocytes were isolated from PBMCs using Dynabead Untouched™ Human Monocytes Kit (Invitrogen) and cultured in DMEM containing 10% fetal calf serum and 1% penicillin/streptomycin (all from Invitrogen).

PBMCs were isolated from buffy coat of healthy donors (25–50 years old) using the Ficoll-Paque (GE Healthcare, CA, USA) standard separation protocol. Informed signed consent was obtained from all donors. PBMCs were culture in RPMI-1640 medium added with FBS 10% and 1% of penicillin/streptomycin solution.

Bone marrow aspirates were collected from healthy donors following Institutional Review Board approval (Uniklinikum, Dresden, Germany) and written informed consent was obtained. The age of the donors was in the range between 22-49 years and gender was mixed. Bone marrow aspirates were diluted 1:5 in PBS. A 20 ml aliquot was layered over a biocoll solution (1.077 g/ml, Biochrom) and centrifuged at 550 g for 30 min at room temperature to separate the mononuclear cells from the anuclear red blood cells. Following centrifugation, the red blood cells were at bottom of the tube and the mononuclear cells, including the desired stem cells, were collected at the interfase above the band of bicoll. To isolate hMSCs, we exploit their adherent properties by seeding the mononuclear cells in a 75 cm^2 flasks. This technique filters out the non-adherent cells, such as the hematopoietic cells, which are a relatively large portion of the bone marrow. The cells were cultured in hMSC medium consisting of Dulbecco's modified Eagle medium (DMEM)-low glucose supplemented with 1% of penicillin/streptomycin solution and 10% fetal calf serum. hMSC cultures were grown at 37°C under a humidified 5% CO_2 atmosphere. Non-adherent cells were removed after 24 h by washing with PBS solution. The medium was changed subsequently every 2 days, and after 2 weeks the cultures were 90% confluent. The cells were used up to four passages. P1–P4 cells were checked routinely by flow cytometry and immunofluorescence microscopy for the presence of the hMSCs defined as CD29+ and CD90+ and CD45- and CD34- (data not shown). The apoptosis assay was performed using Annexin V/PI labeling (Invitrogen,

Carlsbad, CA). Briefly, the cells were incubated for 24 h with increasing doses (2.5, 5, 25, 50 and 100 µg/ml) of GO, CaP, and maGO-CaP or left untreated. The cells were stained with Annexin V/PI staining, incubated for 20 min in the dark and suspended in Annexin V 1× buffer. As positive control, the cells were incubated for 24 h with different concentration (50, 100, and 200 µM) of etoposide, a chemotherapeutic agent, or DMSO (5% and 10%) or cells were incubated for 20 min, before staining, with ethanol at 70% and different concertation of H_2O_2 (0.3%, 0.6% and 3%). The cell fluorescence was measured by flow cytometry (LSR II BD Bioscience) and 50000 to 100000 events were collected.

The CellTiterBlue assay (Promega, Mannheim, Germany) uses dehydrogenase activity and dye resazurin to measure the metabolic capacity of cells as indicator of cell viability. Viable cells retain the ability to reduce resazurin into resorufin, which is highly fluorescent. Nonviable cells rapidly lose metabolic capacity, do not reduce the indicator dye, and do not generate a fluorescent signal. The fluorescent signal from the CellTiter-Blue reagent is proportional to the number of viable cells, therefore, a higher ratio means a higher viability. Cells were seeded in 96-well plates with or without GO, CaP, or maGO-CaP (5, 25, 50 µg/ml). After 24 h the fluorescence intensity was measured using a microplate reader (FluoStar Omega (λ_{ex}: 560 nm, λ_{ex}: 590 nm; BMG).

Immune cell activation assay

PBMCs were seeded in a 12 well plate (1×10^6 cell/well) and treated with increasing doses of GO and maGO-CaP (2.5, 5, 25, 50 µg/ml). The main immune cell populations were stained and the expression of CD69, CD25 and CD80 were analyzed for each population after 24 h.

Monocytes were cultured in a 12 well plate (1×10^6 cell/well) in the presence or absence of increasing doses of GO or maGO-CaP (5, 25, 50 µg/ml). The bacterial endotoxin lipopolysaccharides (LPS, 2 µg/ml; Sigma-Aldrich) was used as positive control of monocyte activation. Concanavalin A (ConA; 10 µg/ml) was used as positive control for T cells B cells

and NK cells. After 24 h of incubation, supernatants were collected to evaluate TNF-α and IL-6 secretion by ELISA kit (Boster Biological Technology), while cells were stained to identify activation markers expression (CD69, CD25 and CD80, eBioscience, San Diego, CA). Staining with fluorochrome-conjugated monoclonal antibodies was performed in the dark for 20 min at 4 °C. After washing, the cells were analyzed by flow cytometry using LSR II (BD Bioscience, Franklin Lakes, NJ).

The monocytes were pre-treated with anti-TLR2 and anti-TLR4 antibodies (Peprotech, Rocky Hill, NJ) for 30 min before incubation with 50 μg/ml of GO and maGO-CaP. The expression of CD69, CD25 and CD80 were evaluated by flow cytometry.

Osteogenesis assay, real-time PCR, osteogenesis array and evaluation of OSM

hMSCs alone (without monocytes) and hMSCs co-cultured with monocytes at a 1:10 ratio were cultured in osteogenic medium: DMEM supplemented with 10 nM dexamethasone, 100 μM ascorbic acid 2-phosphate, and 10 mM β-glycerophosphate. The co-cultures and hMSCs were seeded in 24-well plates in the presence or absence of GO, CaP, and maGO-CaP (50 μg/ml). At day 7, cell lysates were incubated with an ALP substrate buffer (100 mM diethanolamine, 150 mM NaCl, 2 mM $MgCl_2$, and 2.5 mg/ml p-nitrophenylphosphate). Color change was measured at 405 nm via a spectrometer (Fluostar, BMG) and normalized to total the protein concentration measured via BCA method.

To determine the mineral deposition, the cells were fixed at day 14 with 70% ethanol and stained with 40 mM alizarin red S. After washing with distilled water, the plates were dried. The residual bound and stained calcium was then eluted using 100 mM cetylpyridinium chloride and quantified with a spectrometer at 540 nm.

RNA was isolated from co-culture after 14 days of differentiation using Trifast reagent (Invitrogen, Carlsbad, CA) and quantified using Nanodrop spectrophotometer (Peqlab, Germany). Five-hundred nanograms of RNA were reverse transcribed using Superscript II

View Article Online
DOI: 10.1039/C9NR03975A

(Life Technologies, Carlsbad, CA) and the expression of Runx2, Col1a, OCN, BMP6, Axin2, CD44 and LEF1 genes was analyzed using one step plus real-time PCR system from One Step Plus (Applied Biosystems, Foster City, CA). The results were calculated applying the $2^{-\Delta\Delta CT}$ method using β-actin as housekeeping gene. [79]

For the osteogenesis array, cDNA synthesis was performed using Superscript IV Reverse Transcriptase kit (Life Technologies). To identify the expression of 84 osteogenesis-related genes, RT2 Profiler PCR Array (PAHS-026Z, Qiagen Germany) was carried out. Amplifications on plates were performed using a real-time PCR instrument (Applied Biosystems).

Supernatants harvested from co-cultures of hMSCs-monocytes (1:10 ratio) grown in the presence of 50 μg/ml maGO-CaP in osteogenic medium were collected after 7 days to measure secreted OSM levels using a Human OSM/Oncostatin M PicoKine™ ELISA Kit (Bosterbio) according to the manufacturer's instructions. hMSC-monocyte co-cultures maintained alone in osteogenic medium for 7 days represented the control condition.

OSM neutralizing antibody (R&D System) was added or not to the co-cultures at the concentration of 100 ng/ml in the osteogenic medium and alizarin red assay was performed after 14 days.

Co-cultures of hMSCs-monocytes (1:10 ratio) pre-treated with anti-toll like receptor (TLR) 2 and anti-TLR4 antibodies for 30 min before incubation with 50 μg/ml maGO-CaP were additionally analyzed. Alizarin red staining was used to evaluated the bone matrix formation in the presence or the absence of anti-TLR2 and anti-TLR4 after 14 days of treatment with maGO-CaP. The supernatants samples were collected at day 7 and diluted 1:2 with sample diluting buffers. A reference curve was generated using five serial dilutions of appropriate standards.

View Article Online
DOI: 10.1039/C9NR03975A

In vivo study

Thirty 12-weeks-old male C57BL/6 mice were obtained from Janvier (France). The experimental protocol was approved by the Institutional Animal Care Committee and the Landesdirektion Sachsen. To investigate the local effects of graphene in the bone microenvironment, the mice were divided into two groups and were injected intratibially with 20 µl of either 50 µg/ml maGO-Cap in PBS buffer or 20 µl PBS as a negative control. A hole was drilled into the tibia using a 27G × ¾ 0.4 × 19 mm needle and 20 µl of each solution were injected. The mice were sacrificed after one week or four weeks to assess bio-immune compatibility and local bone turnover. The spleen, the lymph nodes, the thymus, and the bone marrow were isolated from mice sacrificed 7 days and 1 month after materials injection. The tissues were mechanical dissociated by gentle trituration and filtered through a cell strainer to create a single cell suspension. The major immune cells populations were identified by flow cytometry according to the expression of specific cells surface markers. Briefly, the cells were washed twice with 0.5% BSA in PBS pH 7.2, then incubated for 20 min in the dark with the following fluorescently labeled antibodies: CD45 for leukocytes, CD3 for T cells, CD4 for T helper, CD8 for T killer, CD11b for myeloid cells, CD11c for dendritic cells and Gr1 for granulocytes. The tibias were analyzed *ex vivo* using microcomputed tomography using a vivaCT40 (Scanco, Switzerland). Scans were taken at a resolution of 10.5 µm and 200 ms integration time. The trabecular bone was contoured by hand and analysis was performed using pre-defined scripts from Scanco. Trabecular bone volume/total volume (BV/TV), trabecular number (Tb.N) and the trabecular thickness (Tb.Th) were evaluated and reported according to international guidelines. [80]

To determine bone formation parameters, mice were injected intraperitoneally with 20 mg/kg calcein (Sigma-Aldrich) two and five days before sacrifice. Dynamic bone histomorphometry was performed as described previously (LIT). Briefly, the tibias were fixed in 4% PBS-buffered paraformaldehyde and dehydrated in an ascending ethanol series. Subsequently, the

View Article Online
DOI: 10.1039/C9NR03975A

bones were embedded in methacrylate and cut into 7 μm sections to assess the fluorescent calcein labels. Unstained sections were analyzed using fluorescence microscopy to determine the mineralized surface/bone surface (MS/BS), the mineral apposition rate (MAR), and the bone formation rate/bone surface (BFR/BS).

The femur of each mouse was fixed in 4% PBS-buffered paraformaldehyde, decalcified for one week using Osteosoft (Merck, Germany), dehydrated using ascending series of ethanol and embedded with paraffin. Bones were cut into 4 μm sections and stained for tartrate-resistant acid phosphatase (TRAP) to identify osteoclasts and osteoblasts. Histomorphometric analysis was performed with the Osteomeasure software (OsteoMetrics, USA) according to international standards. [81]

Supporting Information

Supporting Information is available from the Wiley Online Library or from the author.

Acknowledgements

This work was partly supported by the Centre National de la Recherche Scientique (CNRS), the Agence Nationale de la Recherche (ANR) through the LabEx project Chemistry of Complex Systems (ANR-10-LABX-0026_CSC) (to A. B.), and the International Center for Frontier Research in Chemistry (icFRC). The authors gratefully acknowledge financial support from ANR (ANR-15-GRFL-0001-05), MIUR JTC Graphene 2015 (G-IMMUNOMICS project), European Union HORIZON 2020 research and innovation programme under MSCA RISE 2016 project Carbo-Immap grant no. 734381 and under MSCA IF 2017 project IMM-GNRs. LGD thanks the Italian MIUR (PRIN call 2015, project: 2015TWP83Z). LGD is grateful to Prof. Lorenz Hofbauer for the assistance and the great support. The authors wish to thank Cathy Royer and Valérie Demais for help with TEM

View Article Online
DOI: 10.1039/C9NR03975A

analyses at the "Plateforme Imagerie in vitro" at the Center of Neurochemistry (Strasbourg, France).

Author contributions

L.G.D. with help from A.B and M.R. conceived the idea and supervised the experiments. V.B., G.R. and M.O. implemented the experiments with help from G.F., S.T and C.G. V.B analyzed the data with contributions from M.O, L.G.D., M.R., G.C. and B.Z. V.B., L.G.D., M.R. and A.B. wrote the manuscript with contributions from all authors.

All animal procedures were performed in accordance with the Guidelines for Care and Use of Laboratory Animals of the Technische Universität Dresden and approved by the Animal Ethics Committee of the Free State of Saxony (Landesdirektion Dresden) (protocol no: 24-9168.11-1/12-2017).

Conflict of interest

The authors declare no conflict of interest.

References

[1] F. Loi, L. A. Córdova, J. Pajarinen, T. H. Lin, Z. Yao, S. B. Goodman, *Bone* **2016**, *86*, 119.

[2] C. R. Black, V. Goriainov, D. Gibbs, J. Kanczler, R. S. Tare, R. O. Oreffo, *Curr Mol Biol Rep*. **2015**, *1*, 132.

[3] T. A. Einhorn, L. C. Gerstenfeld, *Nat. Rev. Rheumatol*. **2015**, *11*, 45

[4] J. R. Arron, Y. Choi, *Nature* **2000**, *408*, 535.

[5] H. Takayanagi, *Nat. Rev. Immunol*. **2007,** *7*, 292.

[6] O. M. Omar, C. Granéli, K. Ekström, C. Karlsson, A. Johansson, J. Lausmaa, C. L. Wexell, P. Thomsen, *Biomaterials* **2011**, *32*, 8190.

[7] C. Shi, E. G. Pamer, *Nat. Rev. Immunol.* **2011**, *11*, 762.

[8] C. Schlundt, T. El Khassawna, A. Serra, A. Dienelt, S. Wendler, H. Schell, N. van Rooijen, A. Radbruch, R. Lucius, S. Hartmann, G. N. Duda, K. Schmidt-Bleek, *Bone* **2015**, *106*, 78.

[9] L. Vi, G. S. Baht, H. Whetstone, A. Ng, Q. Wei, R. Poon, S. Mylvaganam, M. Grynpas, B. A. Alman, *J. Bone Miner. Res.* **2015**, *30*, 1090.

[10] M. K. Chang, L. J. Raggatt, K. A. Alexander, J. S. Kuliwaba, N. L. Fazzalari, K. Schroder, E. R. Maylin, V. M. Ripoll, D. A. Hume, A. R. Pettit, *J. Immunol.* **2008**, *181*, 1232.

[11] I. G. Winkler, N. A. Sims, A. R. Pettit, V. Barbier, B. Nowlan, F. Helwani, I. J. Poulton, N. van Rooijen, K. A. Alexander, L. J. Raggatt, J. P. Levesque, *Blood* **2010**, *116*,4815.

[12] G. G. Walmsley, A. McArdle, R. Tevlin, A. Momeni, D. Atashroo, M. S. Hu, A. H. Feroze, V. W. Wong, P. H. Lorenz, M. T. Longaker, D. C. Wan, *Nanomedicine* **2015**, *11*, 1253.

[13] A. Aryaei, A. H. Jayatissa, A. C. Jayasuriya, *J. Biomed. Mater. Res. A*. **2014**, *102*, 2704.

[14] S. I. Roohani-Esfahani, S. Nouri-Khorasani, Z. Lu, R. Appleyard, H. Zreiqat, *Biomaterials* **2010**, *31*, 5498.

[15] T. Chae, H. Yang, V. Leung, F. Ko, T. Troczynski, *J. Mater. Sci. Mater. Med.* **2013**, *24*, 1885.

[16] M. D. Stoller, S. J. Park, Y. W. Zhu, J. H. An, R. S. Ruoff, *Nano Lett*. **2008**, *8,* 3498.

[17] H. J. Jiang, *Small* **2011**, *7*, 2413.

[18]. G. Xin, T. Yao, H. Sun, S. M. Scott, D. Shao, G. Wang, J. Lian. *Science* **2015**, *349*, 1083.

[19] A. H. Castro Neto, F. Guinea, N. M. R. Peres, K. S. Novoselov, A. K. Geim, *Rev. Mod. Phys.* **2009**, *81*, 109.

[20] W.C. Lee, C. H. Lim, H. Shi, L. A. Tang, Y. Wang, C. T. Lim, K. P. Loh, *ACS nano* **2011,** *5*, 7334.

[21] R. Tatavarty, H. Ding, G. Lu, R. J. Taylor, X. Bi, *Chem. Commun. (Camb)* **2014**, *50*, 8484.

[22] N. Dubey, R. Bentini, I. Islam, T. Cao, A. H. Castro Neto, V. Rosa, *Stem Cells Int.* **2015**, *2015,* 804213.

[23] L. Jin, J. H. Lee, O. S. Jin, Y. C. Shin, M. J. Kim, S. W. Hong, M. H. Lee, J. C. Park, D. W. Han, *J. Nanosci. Nanotechnol.* **2015**, *15*, 7966.

[24] M. Zhao, Y. Dai, X. Li, Y. Li, Y. Zhang, H. Wu, Z. Wen, C. Dai, *Mater. Sci. Eng. C. Mater. Biol. Appl.* **2018**, *90*, 365.

[25] C. Dou, N. Ding, F. Luo, T. Hou, Z. Cao, Y. Bai, C. Liu, J. Xu, S. Dong, *Adv Sci (Weinh)* **2017**, *5*, 1700578.

[26] D. Mohammadrezaei, H. Golzar, M. Rezai Rad, H. Rashedi, F. Yazdian, A. Khojasteh L. Tayebi, *J. Biomed. Mater. Re.s A.* **2018**, *106*, 2284.

[27] M. Orecchioni, D. Bedognetti, L. Newman, C. Fuoco, F. Spada, W. Hendrickx, F. M. Marincola, F. Sgarrella, A. F. Rodrigues, C. Ménard-Moyon, G. Cesareni, K. Kostarelos, A. Bianco, L. G. Delogu, *Nat. Commun.* **2017**, *8*, 1109.

[28] M. Orecchioni, C. Ménard-Moyon, L. G. Delogu, A. Bianco, *Adv. Drug Deliv. Rev.* **2016**, *105*, 163.

[29] M. Orecchioni, R. Cabizza, A. Bianco, L. G. Delogu, *Theranostics* **2015**, *5*, 710.

[30] M. Orecchioni, D. A. Jasim, M. Pescatori, R. Manetti, C. Fozza, F. Sgarrella, D. Bedognetti, A. Bianco, K. Kostarelos, L. G. Delogu, *Adv. Healthc. Mater.* **2016**, *5*, 276.

[31] Z. Chen, A. Bachhuka, S. Han, F. Wei, S. Lu, R. M. Visalakshan, K. Vasilev, Y. Xiao, *ACS Nano* **2017**, 11, 4494.

[32] H. D. Kim, S. Amirthalingam, S. L. Kim, S. S. Lee, J. Rangasamy, N.S. Hwang, *Adv. Healthc. Mater.* **2017**, *6*.

[33] H. Wouter, P. Habibovic, M. Epple, M. Bohner, *Materials Today* **2016**, *19*, 69.

[34] F. Bakan, O. Laçin, H. Sarac, *Powder Technol.* **2013**, *233*, 295.

[35] Q. Zhang, Y. Liu, Y. Zhang, H. Li, Y. Tan, L. Luo, C. E. Banks, *Analyst* **2015**, *140*, 5235.

[36] N. R. Wilson, P. A. Pandey, R. Beanland, R. J. Young, I. A. Kinloch, L. Gong, Z. Liu, K. Suenaga, J. P. Rourke, S. J. York, J. Sloan, *ACS Nano* **2009**, *3*, 2547.

[37] A. Bianco, *Angew. Chem. Int. Ed. Engl.* **2013**, *52*, 4986.

[38] M. Orecchioni, D. Bedognetti, F. Sgarrella, F. M. Marincola, A. Bianco, L. G.Delogu, *J. Transl. Med.* **2014**, 12, 138.

[39] T. R. Nayak, H. Andersen, V.S. Makam, C. Khaw, S. Bae, X. Xu, P. L. Ee, J. H. Ahn, B. H. Hong, G. Pastorin, B. Özyilmaz, *ACS Nano* **2011**, *5*, 4670.

[40] N. V. Vallabani, S. Mittal, R. K. Shukla, A. K. Pandey, S. R. Dhakate, R. Pasricha, A. Dhawan, *J. Biomed. Nanotechnol.* **2011**, *7*, 106.

[41] S.M. Kang, T. H. Kim, J. W. Choi, *J. Nanosci. Nanotechnol.* **2012**, *7*, 5185.

[42] X.F. Zhang, S. Gurunathan, *Int J Nanomedicine.* **2016**, *11*, 6635.

[43] G. Y. Chen, D. W. Pang, S. M. Hwang, H. Y. Tuan, Y. C. Hu, *Biomaterials* **2012**, *33*, 418.

[44] J. Qiu, D. Li, X. Mou, J. Li, W. Guo, S. Wang, X. Yu, B. Ma, S. Zhang, W. Tang, Y. Sang, P. R. Gil, H. Liu, *Adv. Healthc. Mater*. **2016**, *5*, 702.

[45] D. C. Zancanela, A. M. Simão, C. G. Francisco, A. N. de Faria, A. P. Ramos, R. R. Gonçalves, E. Y. Matsubara, J. M. Rosolen, P. Ciancaglini, *J. Mater. Sci. Mater. Med.* **2016**, *27*, 71.

[46] H. T. Maecker, J. P. McCoy, R. Nussenblatt, *Nat Rev Immunol.* **2012**, *12*, 191.

[47] G. Finak, M. Langweiler, M. Jaimes, M. Malek, J. Taghiyar, Y. Korin, K. Raddassi, L. Devine, G. Obermoser, M. L. Pekalski, N. Pontikos, A. Diaz, S. Heck, F. Villanova, N. Terrazzini, F. Kern, Y. Qian, R. Stanton, K. Wang, A. Brandes, J. Ramey, N. Aghaeepour, T. Mosmann, R. H. Scheuermann, E. Reed, K. Palucka, V. Pascual, B. B. Blomberg, F. Nestle, R. B. Nussenblatt, R. R. Brinkman, R. Gottardo, H. Maecker, J. McCoy, *Sci Rep.* **2016**, *6*, 20686.

[48] X. Zhi, H. Fang, C. Bao, G. Shen, J. Zhang, K. Wang, S. Guo, T. Wan, D. Cui, *Biomaterials* **2013**, *34*, 5254.

[49] J. Russier, E. Treossi, A. Scarsi, F. Perrozzi, H. Dumortier, L. Ottaviano, M. Meneghetti, V. Palermo, A. Bianco, *Nanoscale* **2013**, *5*, 11234.

[50] P. Guihard, Y. Danger, B. Brounais, E. David, R. Brion, J. Delecrin, C. D. Richards, S. Chevalier, F. Rédini, D. Heymann, H. Gascan, F. Blanchard, *Stem Cells.* **2012**, *30*, 762.

[51] V. Nicolaidou, M. M. Wong, A. N. Redpath, A. Ersek, D.F. Baban, L. M. Williams, A. P. Cope, N. J. Horwood, *PloS one* **2012**, *7*, e39871.

[52] J. L. Millán, M. P. Whyte *Calcif Tissue Int*. **2016**, *98,* 398.

[53] S. Jo, J. Han, Y. L. Lee, S. Yoon, J. Lee, S. Wang, T. Kim *Int J Rheum Dis.* **2018** [Epub ahead of print].

[54] C. Wennberg, L. Hessle, P. Lundberg, S. Mauro, S. Narisawa, U. H. Lerner, J. L. Millán, *J Bone Miner Res.* **2000**, *15*,1879.

[55] N. J. Sheehan, B. M. Slavin, P. R. Kind, J. A. Mathews, *Ann Rheum Dis.* **1983**, *42*, 563.

[56] K. Y. Kang, Y. S. Hong, S. H. Park, J. H. Ju, *Semin Arthritis Rheum*. **2015**, *45*, 202.

[57] S.W. Crowder, D. Prasai, R. Rath, D. A. Balikov, H. Bae, K. Bolotin, H. J. Sung, *Nanoscale* **2013**, *5*, 4171.

[58] J. Li, G. Wang, H. Geng, H. Zhu, M. Zhang, Z. Di, X. Liu, P. K. Chu, X. Wang, *ACS Appl. Mater. Interfaces* **2015**, *7*, 19876.

[59] R.T. Moon, B. Bowerman, M. Boutros, N. Perrimon, *Science*, **2002**, *296*, 1644.

[60] P. Duan, L. F. Bonewald, *Int. J. Biochem. Cell Biol.* **2016**, *77*, 23.

[61] V. Krishnan, H. U. Bryant, O. A. Macdougald, *J Clin Invest.* **2006**, *116,* 1202.

[62] S. Kishida, H. Yamamoto, S. Ikeda, M. Kishida, I. Sakamoto, S. Koyama, A. Kikuchi, *J Biol Chem.* **1998**, *273*, 10823.

[63] S. Shalini, L. Dorstyn, S. Dawar, S. Kumar *Cell Death Differ.* **2015**, *22,* 526.

[64] L. H. Hoeppner, F. J. Secreto, D. F. Razidlo, T. J. Whitney, J. J. Westendorf, *J Biol Chem*. **2011**, *286*, 10950.

[65] E. C. Walker, N. E. McGregor, I. J. Poulton, M. Solano, S. Pompolo, T. J. Fernandes, M. J. Constable, G. C. Nicholson, J. G. Zhang, N. A. Nicola, M. T. Gillespie, T. J. Martin, N. A. Sims, *J Clin Invest.* **2010**, *120*, 582.

[66] H. Y. Song, E. S. Jeon, J. I. Kim, J. S. Jung, J. H. Kim, *J Cell Biochem.* **2007**, *101,* 1238.

[67] T. J. Fernandes, J. M. Hodge, P. P. Singh, D. G. Eeles, F. M. Collier, I. Holten, P. R. Ebeling, G. C. Nicholson, J. M. Quinn, *PLoS One.* **2013**, *8*, e73266.

[68] P. Guihard, M. A. Boutet, B. Brounais-Le Royer, A. L. Gamblin, J. Amiaud, A. Renaud, M. Berreur, F. Rédini, D. Heymann, P. Layrolle, F. Blanchard, *Am. J. Pathol.* **2015**, *185*, 765e775.

[69] S. W. Cho, F. N. Soki, A. J. Koh, M. R. Eber, P. Entezami, S. I. Park, N. van Rooijen, L. K. McCauley, *Proc Natl Acad Sci USA* **2014**, *111*, 1545.

[70] C. H. Côté, P. Bouchard, N. van Rooijen, D. Marsolais, E. Duchesne, *BMC Musculoskelet Disord.* **2013**, *14*, 359.

[71] J. Pajarinen, T. Lin, E. Gibon, Y. Kohno, M. Maruyama, K. Nathan, L. Lu, Z. Yao, S. B. Goodman. *Biomaterials.* **2018**, *S0142-9612*, 30834-7.

[72] K. Takeda, T. Kaisho, S. Akira, *Annu. Rev. Immunol.* **2003**, *21*, 335.

[73] J. Ma, R. Liu, X. Wang, Q. Liu, Y. Chen, R. P. Valle, Y. Y. Zuo, T. Xia, S. Liu, *ACS Nano* **2015**, *9*, 10498.

[74] G. Y. Chen, H. J. Yang, C. H. Lu, Y. C. Chao, S. M. Hwang, C. L. Chen, K. W. Lo, L. Y. Sung, W. Y. Luo, H. Y. Tuan, Y. C. Hu, *Biomaterials* **2012**, *33*, 6559.

[75] G. Qu, S. Liu, S. Zhang, L. Wang, X. Wang, B. Sun, N. Yin, X. Gao, T. Xia, J. J. Chen, G. B. Jiang, *ACS Nano*, **2013**, *7*, 5732.

[76] J. Russier, V. León, M. Orecchioni, E. Hirata, P. Virdis, C. Fozza, F. Sgarrella, G. Cuniberti, M. Prato, E. Vázquez, A. Bianco, L. G. Delogu, *Angew. Chem. Int. Ed. Engl*. **2017**, *56*, 3014.

[77] S. P. Kastl, W. S. Speidl, C. Kaun, K. M. Katsaros, G. Rega, T. Afonyushkin, V. N. Bochkov, P. Valent, A. Assadian, G. W. Hagmueller, M. Hoeth, R. de Martin, Y. Ma, G. Maurer, K. Huber, J. Wojta *Arterioscler Thromb Vasc Biol.* **2008**, *28*, 498.

[78] S. P. Kastl, W. S. Speidl, K. M. Katsaros, C. Kaun, G. Rega, A. Assadian, G. W. Hagmueller, M. Hoeth, R. de Martin, Y. Ma, G. Maurer, K. Huber, J. Wojta, *Blood.* **2009**, *114*,2812.

[79] M. W. Pfaffl, *Nucleic. Acids Res*. **2001,** *29*, e45.

[80] M. L. Bouxsein, S. K. Boyd, B. A. Christiansen, R. E. Guldberg, K. J. Jepsen, R. Müller, *J. Bone Miner. Res.* **2010**, *25*, 1468.

[81] S. Hengsberger, P. Ammann, B. Legros, R. Rizzoli, P. Zysset, *Bone* **2005**, *36*, 134

Figures

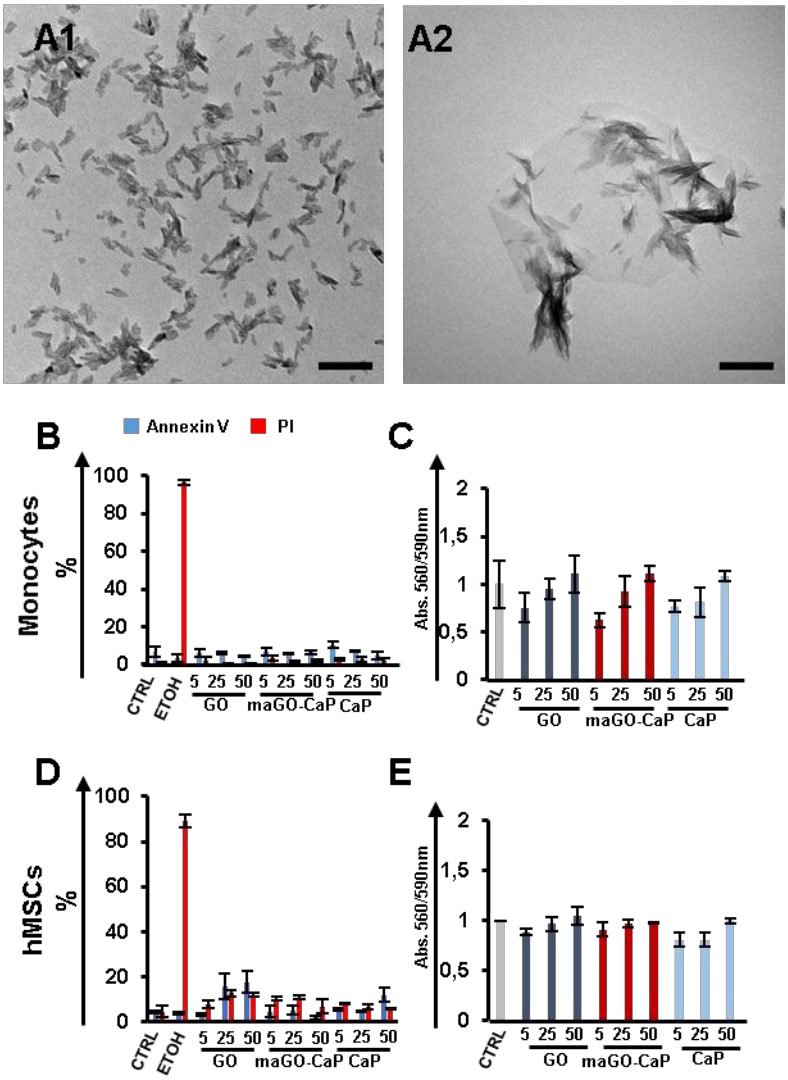

Figure 1. Morphology of maGO-CaP and cell viability. A1) and A2) TEM images of mature CaP and maGO-CaP (scale bar: 200 nm). B) and C) Monocytes were isolated from PBMCs and cultured in presence or absence of increasing doses of GO, maGO-CaP and CaP (5, 25, 50 µg/ml) for 24 h or left untreated. B) Viability was assessed by Annexin V/PI staining, and C) by CellTiter-Blue assay. D) and E) hMSCs were isolated from bone marrow of healthy donors and treated with increasing doses of GO, maGO-CaP and CaP (5, 25, 50 µg/ml) for 24 h or left untreated. Viability of hMSCs was measured by D) Annexin V/PI staining and E) CellTiter Blue assay.

View Article Online
DOI: 10.1039/C9NR03975A

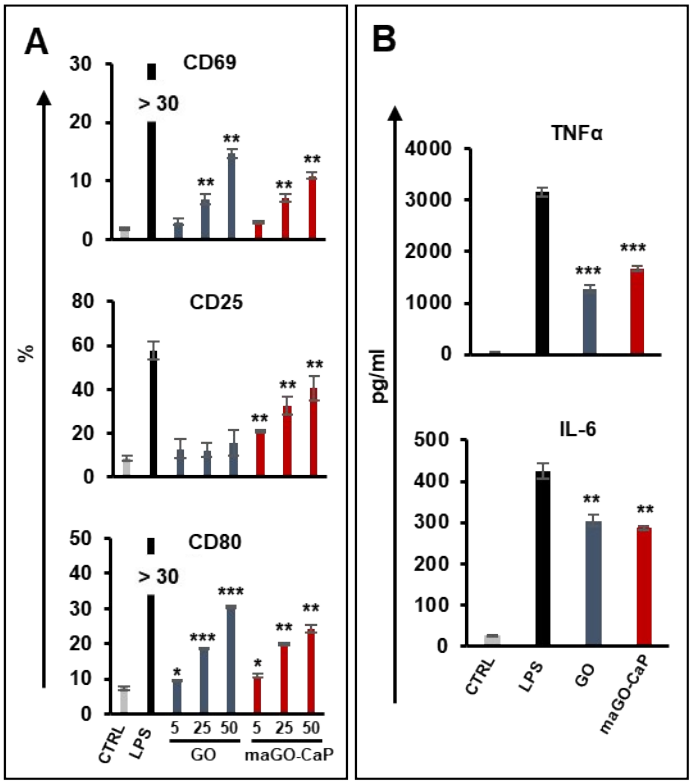

Figure 2. Monocyte activation. Monocytes were treated for 24 h with increasing doses of GO and maGO-CaP (5, 25, 50 µg/ml) or left untreated. A) The samples were analyzed by flow cytometry using several activation markers: CD69, CD25 and CD80. B) Cells were treated with 50 µg/ml of GO or maGO-CaP or left untreated, TNFα and IL-6 secretion was evaluated by ELISA. LPS (2 µg/ml) was used as positive control. Data were analyzed using Student's t test, *=p value<0.05, **=p value<0.01, ***=p value<0.001.

View Article Online
DOI: 10.1039/C9NR03975A

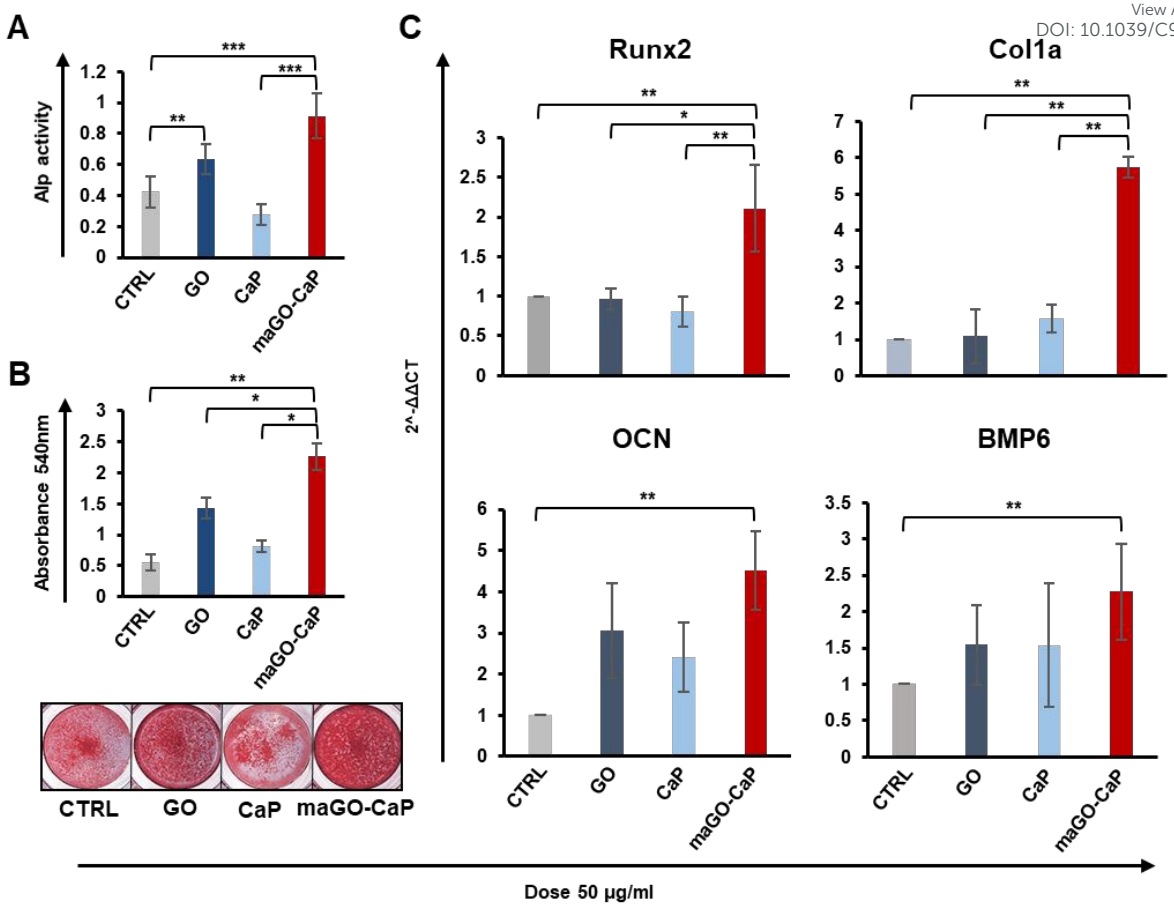

Figure 3. Osteogenic differentiation of hMSCs. A co-culture of hMSCs and monocytes was performed in 1:10 ratio. The cells were left untreated or incubated at 50 µg/ml of each material. A) ALP activity was quantified after 7 days of incubation. Color change was measured at 405 nm via a spectrometer and normalized to the total protein concentration measured via BCA method. B) Alizarin red assay was performed to visualize the bone matrix formation at day 14. The plate was scanned, visualizing the stained calcium. The residual bound and stained calcium was then eluted using 100 mM cetylpyridinium chloride and quantified with a spectrometer at 540 nm. C) The main genes involved in osteoblast differentiation were detected by Real-Time PCR: RUNX2, Col1a, OCN and BMP6. Data were analyzed using ANOVA test and Student's t test, *=p value<0.05, **= p value<0.01, ***=p value<0.001.

View Article Online
DOI: 10.1039/C9NR03975A

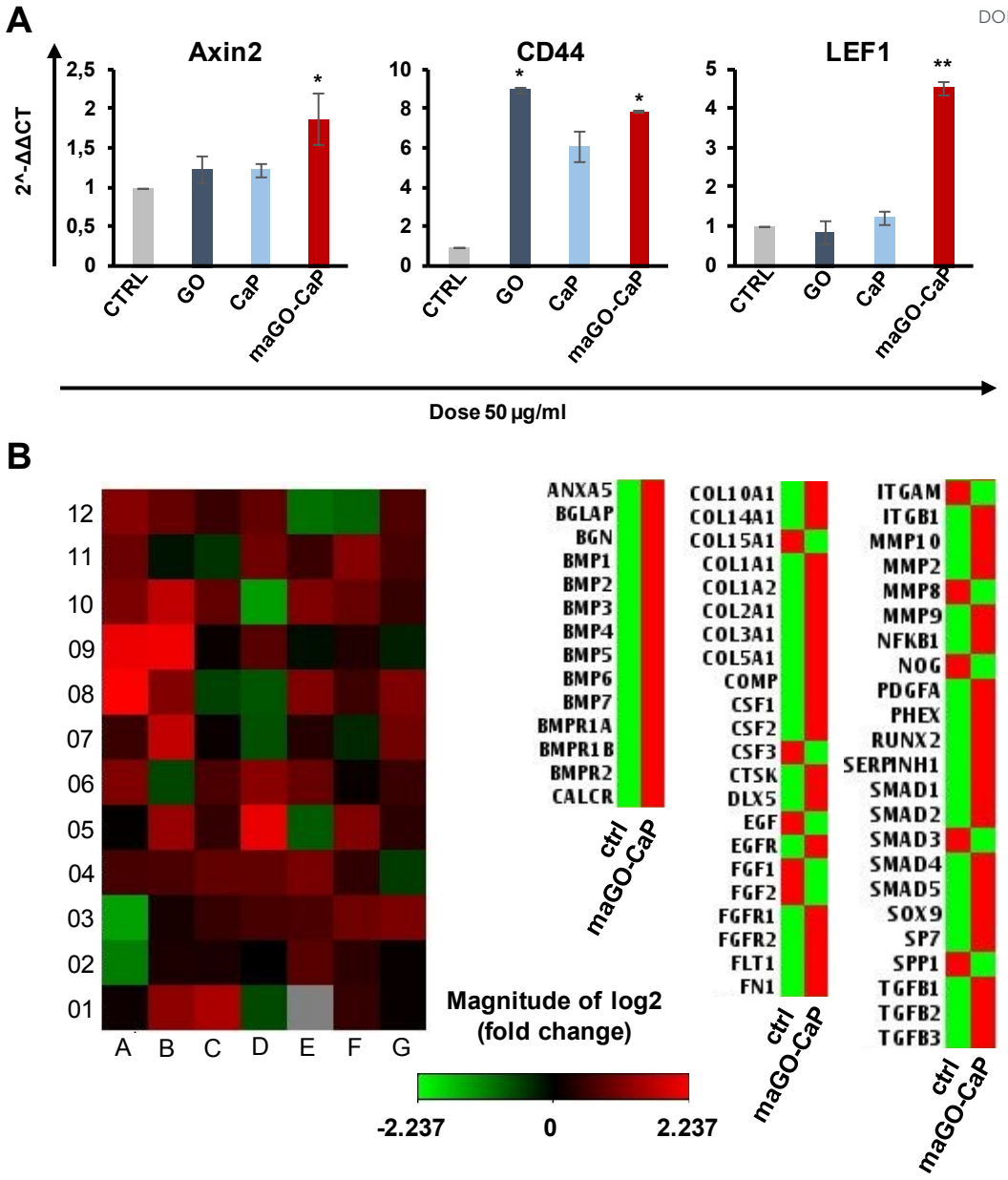

Figure 4. Osteogenesis pathways. A co-culture of hMSC and monocytes (1:10) was incubated for 14 days with 50 µg/ml of GO, CaP and maGO-CAP. A) The main genes involved in the Wnt pathway were analyzed by Real-Time PCR. B) Expression array for osteogenic genes. Data are reported as mean of experiments carried out at least in triplicate. (Left) Genes are displayed for fold-change variations compared to the controls and colored by their standardized expression value (red= high expression; green= low expression). (Right) Heat-map detail showing the osteo-differentiation transcript up-regulated by maGO-CaP. Data were analyzed using Student's t test, *=p value<0.05, **= p value<0.01.

View Article Online
DOI: 10.1039/C9NR03975A

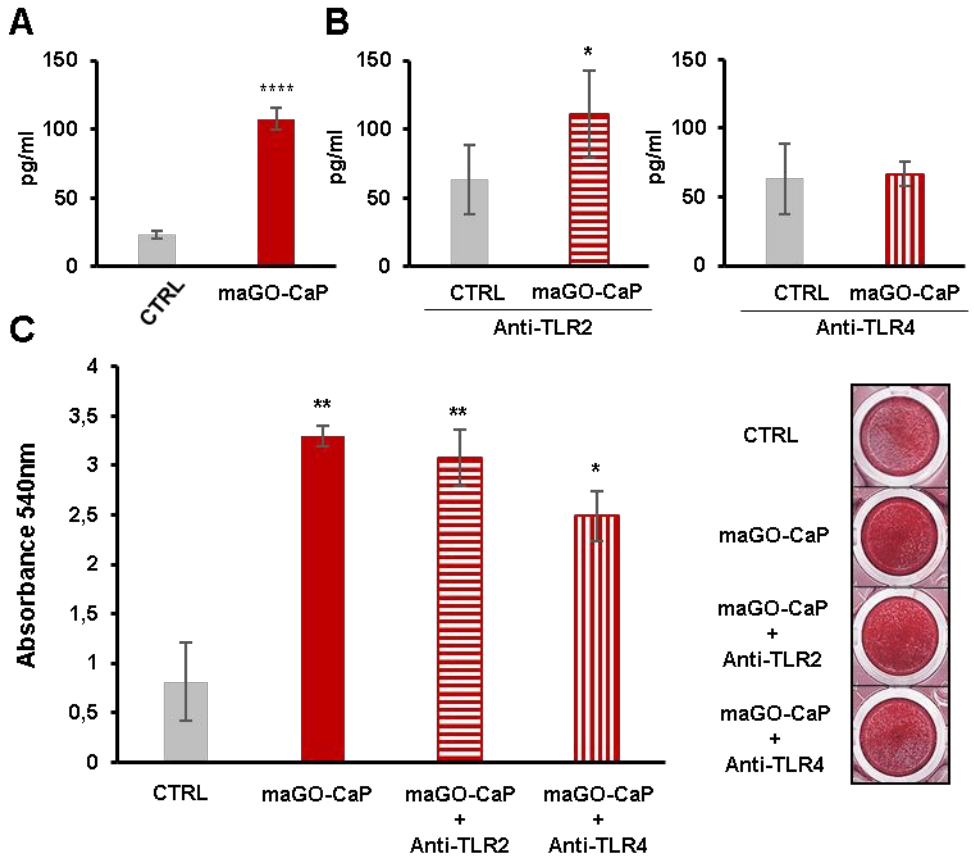

Figure 5. OSM assay and osteogenesis mechanism. A) hMSC-monocyte co-cultures were grown in the presence of 50 µg/ml maGO-CaP or left untreated for 7 days. The collected supernatant media were analyzed by ELISA to evaluate OSM levels. B) Antibodies blocking TLR2 and TLR4 were incubated with hMSC-monocyte co-cultures, followed by treatment with 50 µg/ml maGO-CaP for 7 days. OSM secretion was quantified by ELISA in the cell culture supernatants. C) hMSCs were co-cultured with monocytes, pre-treated or left untreated with anti-TLR2 and anti-TLR4 and incubated with maGO-CaP for 14 days. Alizarin red staining was performed to visualize the formation of the bone matrix. Test t assuming equal variance between test conditions and control condition (*=p value<0.05, **= p value<0.01, ***= p value<0.001, ****=p value<0.0001).

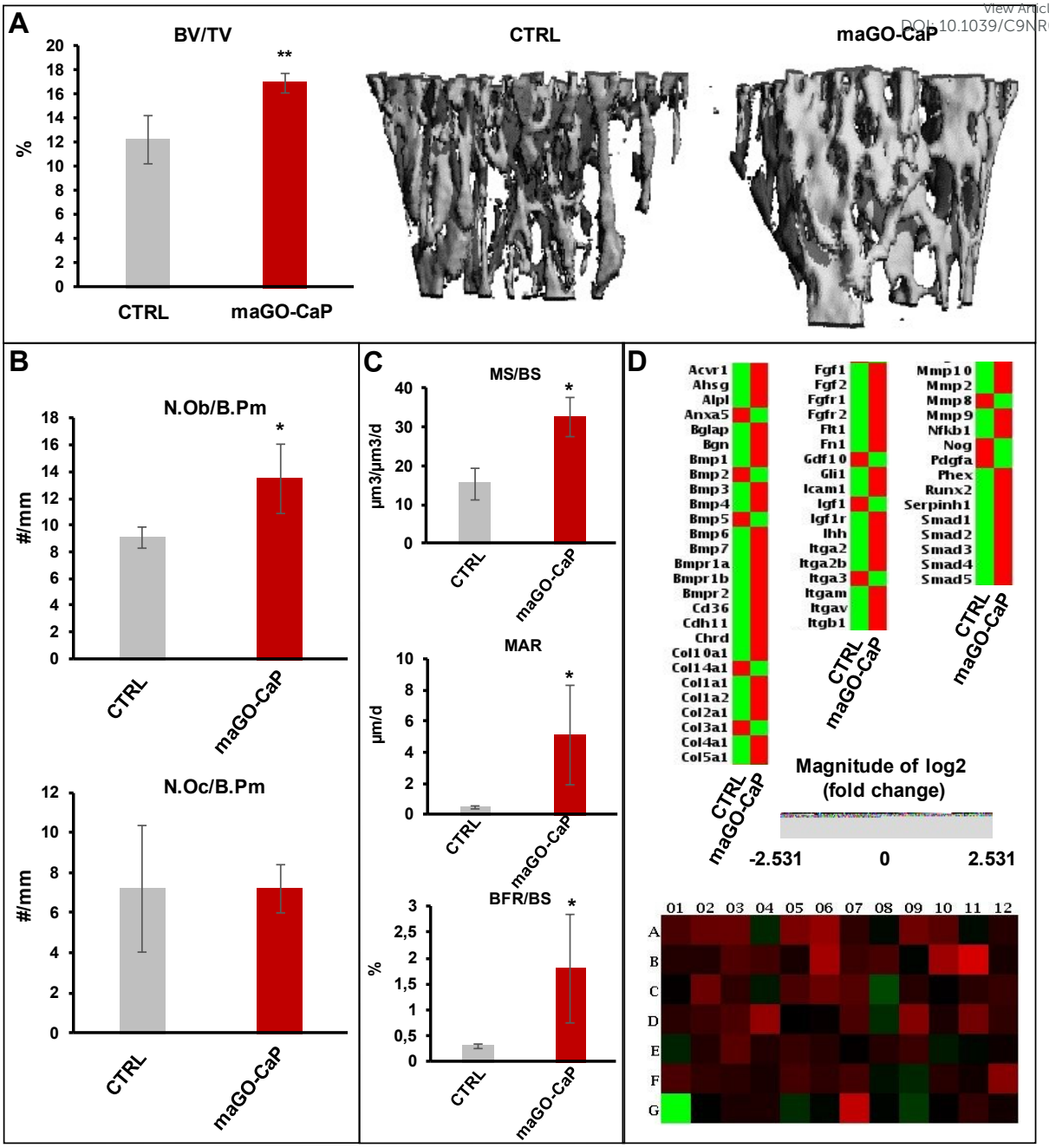

Figure 6. *In vivo* bone formation. Ten mice were injected intratibially with 20 µl of 50 µg/ml maGO-Cap or 20 µl PBS, as a negative control. A) The tibias (5 per group) were analyzed by µCT. Scans were taken at a resolution of 10.5 µm and 200 ms integration time. A) Left, the histogram shows the ratio between trabecular bone volume and total volume (BV/TV). Right, µCT image of untreated tibia (CTRL) and one month after treatment with maGO-CaP. B) Mice femurs were used for histology analysis. Tartrate-resistent acid phosphatase (TRAP) staining was performed. The number (#) of osteblasts (top) per

View Article Online
DOI: 10.1039/C9NR03975A

perimeter bone and the number of osteoclasts (bottom) per perimeter bone were determined. C) Mice were injected with 20 mg/kg calcein 2 and 5 days before sacrifice. Unstained sections were analyzed using fluorescence microscopy to determine the mineralized surface/bone surface (MS/BS), the mineral apposition rate (MAR), and the bone formation rate/bone surface (BFR/BS). D) Heat map of the genes after intratibial injection of the mice with maGO-CaP and PBS buffer as control. Data are reported as mean of experiments carried out in triplicate. Genes are displayed for fold-change variations compared to the controls and colored by their standardized expression value (red: high expression; green: low expression). Heat-map detail showing the osteo-differentiation transcript up-regulated by maGO-CaP. Data were analyzed using ANOVA test and Student's t test, *= p value<0.05, **= p value<0.01, ***= p value<0.001, ****=p value<0.0001.

Graphical abstract.

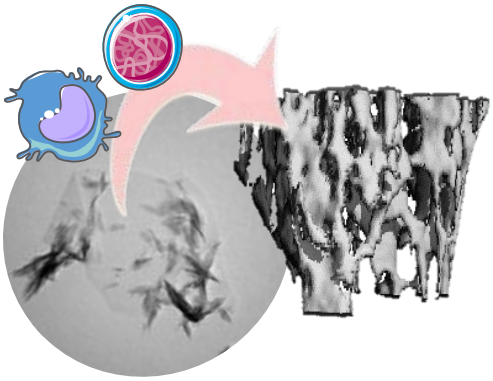

Stimulation of bone formation by monocyte-activator functionalized graphene oxide *in vivo*

Valentina Bordoni[1#], Giacomo Reina[2#], Marco Orecchioni[1#], Giulia Furesi[1,3], Stefanie Thiele[3], Chiara Gardin[4], Barbara Zavan[4], Gianaurelio Cuniberti[5], Alberto Bianco[2], Martina Rauner[3*], and Lucia G. Delogu[1,6,7*]*

[1]University of Sassari, Sassari, Italy, [2]University of Strasbourg, CNRS, Immunology, Immunopathology and Therapeutic Chemistry, UPR 3572 Strasbourg, France, [3]TU Dresden Medical Center, Dresden, Germany, [4]Department of Biomedical Sciences University of Padova, Padova, Italy, [5]Max Bergmann Center of Biomaterials and Institute for Materials Science, Dresden University of Technology, Dresden, Germany, [6]Center for Advancing Electronics Dresden, TU Dresden, Dresden, Germany, [7]Fondazione Istituto di Ricerca Pediatrica Città della Speranza, Padova, Italy.